

First-principles study on structural, electronic, and superconducting properties of Laves-phase alloy $HfZn_2$ under pressure

Xiao Ma(马晓), Tao Wang(王涛), Jianfeng Wen(文剑锋), Zhenwei Zhou(周振玮), and Hongyu Zhu(朱红玉)
Citation: Chin. Phys. B, 2025, 34 (**8**): 086108. DOI: 10.1088/1674-1056/ade5a1
http://cpb.iphy.ac.cn; http://iopscience.iop.org/cpb

What follows is a list of articles you may be interested in

Morphology-tuned phase transition of MnO_2 nanorods under high pressure

Xue-Ting Zhang(张雪婷), Chen-Yi Li(李晨一), Hui Tian(田辉), Xin-Yue Wang(王心悦), Zong-Lun Li(李宗伦), and Quan-Jun Li(李全军)
Chin. Phys. B, 2025, 34 (**6**): 066105. DOI: 10.1088/1674-1056/adc192

Layer-dependent structural stability and electronic properties of $CrPS_4$ under high pressure

Jian Zhu(朱健), Dengman Feng(冯登满), Liangyu Wang(王亮予), Liang Li(李亮), Fangfei Li(李芳菲), Qiang Zhou(周强), and Yalan Yan(闫雅兰)
Chin. Phys. B, 2025, 34 (**6**): 066102. DOI: 10.1088/1674-1056/adc65f

Well defined phase boundaries and superconductivity with high T_c in PbSe single crystal

Jiawei Hu(胡佳玮), Yanghao Meng(孟养浩), He Zhang(张赫), Wei Zhong(钟韦), Hang Zhai(翟航), Xiaohui Yu(于晓辉), Binbin Yue(岳彬彬), and Fang Hong(洪芳)
Chin. Phys. B, 2025, 34 (**4**): 046102. DOI: 10.1088/1674-1056/adb272

First-principles insights into the high-pressure stability and electronic characteristics of molybdenum nitride

Tao Wang(王涛), Ming-Hong Wen(温铭洪), Xin-Xin Zhang(张新欣), Wei-Hua Wang(王伟华), Jia-Mei Liu(刘佳美), Xu-Ying Wang(王旭颖), and Pei-Fang Li(李培芳)
Chin. Phys. B, 2025, 34 (**3**): 036104. DOI: 10.1088/1674-1056/adab66

First-principles study of structural and electronic properties of multiferroic oxide Mn_3TeO_6 under high pressure

Xiao-Long Pan(潘小龙), Hao Wang(王豪), Lei Liu(柳雷), Xiang-Rong Chen(陈向荣), and Hua-Yun Geng(耿华运)
Chin. Phys. B, 2024, 33 (**7**): 076102. DOI: 10.1088/1674-1056/ad3ef6

SPECIAL TOPIC — Structures and properties of materials under high pressure

First-principles study on structural, electronic, and superconducting properties of Laves-phase alloy $HfZn_2$ under pressure

Xiao Ma(马晓)[1], Tao Wang(王涛)[2], Jianfeng Wen(文剑锋)[2], Zhenwei Zhou(周振玮)[2], and Hongyu Zhu(朱红玉)[2,†]

[1] *College of Material Science and Engineering, Guilin University of Technology, Guilin* 541004, *China*

[2] *College of Physics and Electronic Information Engineering, Guilin University of Technology, Guilin* 541006, *China*

(Received 30 May 2025; revised manuscript received 13 June 2025; accepted manuscript online 18 June 2025)

Laves-phase are among the most abundant groups of alloys with chemical formula AB_2, known for their high-temperature strength and potential application in hydrogen storage. The Laves-phase generally acts as a strengthening agent, which enhances the strength and durability of alloys at extreme conditions. Consequently, the properties of Laves-phase alloys at extreme conditions attract wide attention. In this study, we investigated the high-pressure phase diagram of Laves-phase alloy $HfZn_2$, and discovered a phase transition from $C15$ (space group $Fd\bar{3}m$) phase to $C14$ (space group $P6_3/mmc$) phase at a pressure above 20 GPa. Based on *ab initio* simulations, the mechanical, chemical bonding and superconducting properties of high-pressure phase $HfZn_2$ were predicted. The ratio of bulk modulus to shear modulus (B/G), a key indicator of mechanical properties in alloys, increases from 1.86 to 4.09 within the pressure range of 50–250 GPa, indicating excellent ductility of the $C14$ phase of $HfZn_2$ under high pressure. Additionally, Zn gains approximately 0.43 electron from Hf at 10 GPa, and the superconducting critical temperature of $HfZn_2$ is estimated to be around 0.55 K at 50 GPa. Given that both $C14$ and $C15$ phases are common structures in Laves-phase alloys, elucidating the high-pressure behaviors of $C14$ and $C15$ phases of $HfZn_2$ will enhance the fundamental understanding of properties and potential applications at extreme conditions of Laves-phase alloys.

Keywords: Laves-phase alloy, high pressure, phase transition, density function theory

PACS: 61.50.Ks, 31.15.E, 71.20.Be

DOI: 10.1088/1674-1056/ade5a1 **CSTR:** 32038.14.CPB.ade5a1

1. Introduction

Laves-phase intermetallic compounds, formed by main group metallic elements and transition metals, exhibit a variety of crystal structures, including the cubic $C15$ ($MgCu_2$) structure, hexagonal $C14$ ($MgZn_2$) structure, or dihexagonal $C36$ ($MgNi_2$) structure. These compounds have recently garnered renewed interest within the technological and scientific communities due to their intriguing properties and potential applications.[1,2] For instance, Laves-phase ZrX_2 (X = V, Cr, Mn, Fe, Co, Ni) and $C14$-type $ZrMn_2H_3$ compounds are promising candidate materials for hydrogen storage.[3] The cubic Laves compound $ZrZn_2$ was studied both experimentally and theoretically, with superconducting critical temperature $T_c \approx 1$ K.[4] Moreover, the elastic constants of some Laves-phase compounds have been studied by a number of theoretical investigations. For example, the elastic properties of $C15$ Laves-phases HfV_2, ZrV_2, and $Hf_xZr_{1-x}V_2$ exhibit an anomalous temperature dependence.[5] Similarly, the cubic Laves-phase materials $Hf_{25}V_{60}Nb_{15}$, TaV_2, $TaV_2H(D)_x$, and $ZrCr_2$ also show anomalous elastic properties.[6] Due to the potential application of Laves-phase alloys at extreme conditions, the mechanical properties of Laves-phase alloys at pressure attract wide interest.

Up to now, the $C15$ Laves-phase structure of $HfZn_2$ has widely attracted both experimental and theoretical attention.[7,8] The elastic and thermodynamic properties of $HfZn_2$ were studied, and the results demonstrate good agreement with experimental data.[7] The optical properties of $HfZn_2$ were investigated, which show that it is a good coating material with high reflectivity up to 16 eV in the visible-ultraviolet region.[9] In 2017, the superconductivity of $HfZn_2$ was reported with superconducting critical temperature $T_c \approx 0.05$ K. A recent work reported the structural, elastic, electronic, vibrational and thermodynamic properties of $C15$ $HfZn_2$ up to 100 GPa.[10] However, the information on phase transitions, electronic properties, chemical bonding, dynamical properties and superconductivity of $HfZn_2$ under pressure is absent. Therefore, great attention is needed to explore the high-pressure structures and properties of $HfZn_2$. Such studies would not only enhance our fundamental understanding of this material but also potentially unlock new applications in extreme environments.

In this work, we discovered a new $C14$ Laves-phase $HfZn_2$ with the space group $P6_3/mmc$ in the pressure range 20–275 GPa. We investigated the mechanical, chemical bonding and superconducting properties of the new high-pressure

†Corresponding author. E-mail: zhuhy@glut.edu.cn

© 2025 Chinese Physical Society and IOP Publishing Ltd. All rights, including for text and data mining, AI training, and similar technologies, are reserved.

phase of $HfZn_2$ based on *ab initio* simulations. According to the Pugh criterion, the $C14$ Laves-phase $HfZn_2$ was identified with high ductility. Zn gains electrons from Hf in the $C14$ Laves-phase $HfZn_2$ crystal. And $HfZn_2$ was predicted to be a superconductor with a critical temperature of about 0.55 K under pressures. Our results provide a theoretical perspective for understanding the properties of $HfZn_2$ under extreme conditions.

2. Computational methods

The crystal structure prediction for $HfZn_2$ was performed at the pressure range of 0–300 GPa with 1–4 formula units, through the CALYPSO and USPEX codes.[11,12] Such methods have been manifested by successfully employed in high-pressure phases of various systems.[13] The structural relaxations and electronic structure calculations were carried out by using the first-principles method through the Vienna *ab initio* simulation package (VASP) codes.[14–16] PBE (Perdew–Burke–Ernzerhof)[17] in generalized gradient approximation (GGA) was used as the exchange–correlation functional. The $5d^26s^2$ for Hf and $3d^{10}4s^2$ for Zn were considered as valence electrons, respectively. To obtain an accurate result, the energy cutoff was set to 600 eV, and the Brillouin-zone sampling mesh for the Monkhorst–Pack k-point was used $2\pi \times 0.025$ Å^{-1}. The phonon dispersion of the thermodynamically stable structures was calculated to confirm the dynamic stability by using a supercell approach as implemented in the Phonopy code.[18] The electron–phonon coupling (EPC) calculations were implemented by using the Quantum ESPRESSO[19] package with a 90 Ry kinetic energy cutoff and a 360 Ry charge density cutoff. For $Fd\bar{3}m$ phase, a $16 \times 16 \times 16$ k-point grid was used for Brillouin zone integration in electronic calculations and EPC matrix elements were calculated in a $4 \times 4 \times 4$ q-point grid. For $P6_3/mmc$ phase, a $12 \times 12 \times 8$ k-point grid was used for Brillouin zone integration in electronic calculations and EPC matrix elements were calculated in a $3 \times 3 \times 2$ q-point grid.

3. Results and discussion

3.1. Thermodynamic, dynamic and mechanical stability of predicted structures

The crystal structures were predicted to exhibit the $Fd\bar{3}m$, $P6_3/mmc$, and $P2_1/m$ space groups within the pressure range of 0–300 GPa. Figure 1(a) illustrates the calculated enthalpies of the predicted structures relative to the enthalpy of $Fd\bar{3}m$ phase as a function of pressure. The $Fd\bar{3}m$ phase has the lowest enthalpy among all other candidates from 0 to 20 GPa, indicating it is the thermodynamic ground state. Upon compression, a hexagonal structure becomes more thermodynamically favored up to 275 GPa. Beyond this pressure, it decomposes to the elements Hf and Zn. The crystal structures of $Fd\bar{3}m$ and $P6_3/mmc$ phases are depicted in Figs. 2(a) and 2(b), respectively. At ambient pressure, we obtain the cubic $C15$ structure with space group $Fd\bar{3}m$, which is in good agreement with previous studies.[7,8] Interestingly, we observe a hexagonal structure with $P6_3/mmc$ space group at 100 GPa, in which the occupations of Hf and Zn are the same as that in $C14$ phase of $MgZn_2$. Hf atoms occupy $4f$ and Zn atoms occupy $2a$ and $6h$, indicating this structure belongs to the family of $C14$ Laves-phase. Detail parameters of the structures are shown in the supporting information. The calculated equations of state (EOS) for the $Fd\bar{3}m$ and $P6_3/mmc$ are shown in Fig. 1(b). The volume change is discontinuous with 0.59% at $Fd\bar{3}m$-to-$P6_3/mmc$ transition point, which suggests the transition is the first-order nature.

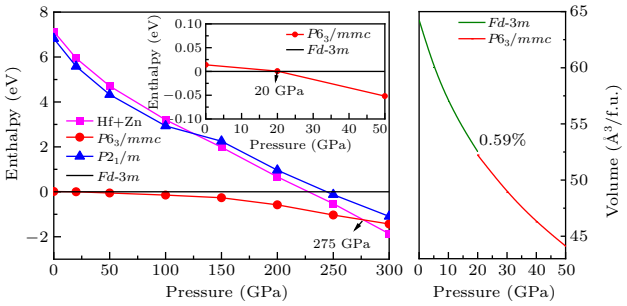


Fig. 1. (a) Calculated enthalpies of the predicted structures of $HfZn_2$ relative to enthalpy of $Fd\bar{3}m$ phase as a function of pressure. (b) Equation of state curves of $HfZn_2$ with $Fd\bar{3}m$ and $P6_3/mmc$ space symmetry.

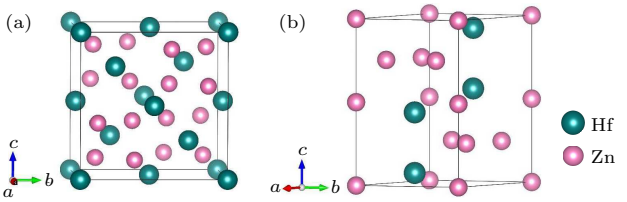


Fig. 2. The crystal structures of (a) $Fd\bar{3}m$ and (b) $P6_3/mmc$ phases of $HfZn_2$.

Then the phonon band structure along highly symmetrical directions within the Brillouin zone and projected phonon density of states (PHDOS) for two phases of $HfZn_2$ were calculated to investigate the dynamical stability, which is an important condition for judging the stability of the structure. The dynamic properties of $Fd\bar{3}m$ at 10 GPa and $P6_3/mmc$ at 200 GPa were studied, as shown in Fig. 3. The absence of imaginary frequency throughout the Brillouin zone confirms the dynamical stability of both phases. Additionally, because hafnium is much heavier than zinc, the vibrational frequency of Hf atom is obviously lower than that of Zn atom. Therefore, the low-frequency bands primarily originate from the heavier Hf atoms, while lighter Zn atoms dominate higher-frequency modes.

Mechanical stability is another important criterion for assessing the stability of crystal structures. To investigate the

mechanical properties of the $C15$ and $P6_3/mmc$ phases, we calculated their elastic constants, as presented in Table 1. In addition, for mechanically stable crystals, the independent elastic constants C_{ij} must satisfy the Born–Huang stability criteria.[20] In the cubic phase, there are three independent components (C_{11}, C_{44}, and C_{12}), and the mechanical stability criteria are defined by the following equations:

$$C_{11} > 0, \tag{1}$$

$$C_{44} > 0, \tag{2}$$

$$C_{11} > |C_{12}|, \tag{3}$$

$$C_{11} + 2C_{12} > 0. \tag{4}$$

In the hexagonal phase, there are five independent components (C_{11}, C_{33}, C_{44}, C_{12}, and C_{13}). The criteria for mechanical stability are given by the three equations:

$$C_{44} > 0, \tag{5}$$

$$C_{11} > |C_{12}|, \tag{6}$$

$$(C_{11} + 2C_{12})C_{33} > 2{C_{13}}^2. \tag{7}$$

It is obvious that the elastic constants of $Fd\bar{3}m$ and $P6_3/mmc$ satisfy the above conditions, indicating that they are mechanically stable.

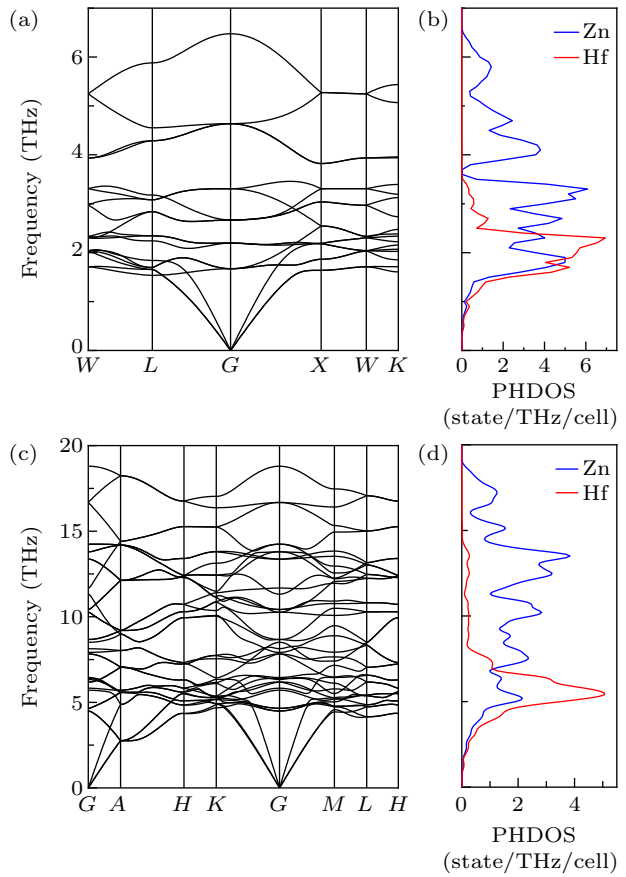


Fig. 3. (a) Phonon band structure and (b) projected phonon density of states of $HfZn_2$ with $Fd\bar{3}m$ space group. (c) Phonon band structure and (d) projected phonon density of states of $HfZn_2$ with $P6_3/mmc$ space group.

Table 1. Elastic constants for the structure of $Fd\bar{3}m$ at 10 GPa and $P6_3/mmc$ at 200 GPa.

	C_{11}	C_{12}	C_{44}	C_{13}	C_{33}
$Fd\bar{3}m$	1109.34	418.48	364.31		
$P6_3/mmc$	9622.88	4122.11	1319.47	4818.49	4768.00

3.2. Elastic properties

Previous studies have extensively investigated the elastic properties of the cubic $C15$ phase of $HfZn_2$. In this work, we mainly focused on the $C14$ Laves-phase. Figure 4 shows the elastic constants, bulk modulus (B_V, B_R, B), shear modulus (G_V, G_R, G), Young's modulus E, the Pugh criterion (B/G) and Poisson's ratio as functions of pressure. These physical quantities are obtained by the following equations for the hexagonal phase:[21]

$$|B_V| = \frac{1}{9}[2(C_{11} + C_{12}) + 4C_{13} + C_{33}], \tag{8}$$

$$G_V = \frac{1}{30}[M + 12C_{44} + 12C_{66}], \tag{9}$$

$$B_R = \frac{C^2}{M}, \tag{10}$$

$$G_R = \frac{5C^2C_{44}C_{66}}{2[3B_VC_{44}C_{66} + C^2(C_{44} + C_{66})]}, \tag{11}$$

$$M = C_{11} + C_{12} + 2C_{33} - 4C_{13}, \tag{12}$$

$$C^2 = (C_{11} + C_{12})C_{33} - 2{C_{13}}^2. \tag{13}$$

In terms of the Voigt–Reuss–Hill approximations,[22]

$$M_H = \frac{1}{2(M_R + M_V)}, \quad M = B, G. \tag{14}$$

Young's modulus E and Poisson's ratio ν are given by the following equations:[23]

$$E = \frac{9BG}{3B + G}, \tag{15}$$

$$\nu = \frac{3B - 2G}{2(3B + G)}. \tag{16}$$

It is observed that the elastic constants C_{11}, C_{12}, C_{13}, C_{33} and C_{66} increase with applied pressure. In contrast, C_{44} initially increases in the pressure range of 50–150 GPa, but subsequently decreases in the range of 150–250 GPa (Fig. 4(a)). These variations in the elastic constants result in corresponding changes in the moduli, as depicted in Figs. 4(b) and 4(c). It is known that if the Pugh criterion (B/G) value is larger than 1.75, the material behaves in a ductile manner, otherwise, it behaves in a brittle manner. The B/G values increase from 1.86 to 4.09 over the pressure range of 50–250 GPa (Fig. 4(d)), which indicates that the $C14$ Laves-phase of $HfZn_2$ has good ductility. Poisson's ratio is another way to evaluate the mechanical response of materials to external stress. The high and low values of Poisson's ratio correspond to good ductility and brittleness, respectively. As shown in Fig. 4(d), the Poisson's ratio values range from 0.27 to 0.39, consistent with the B/G ratios.

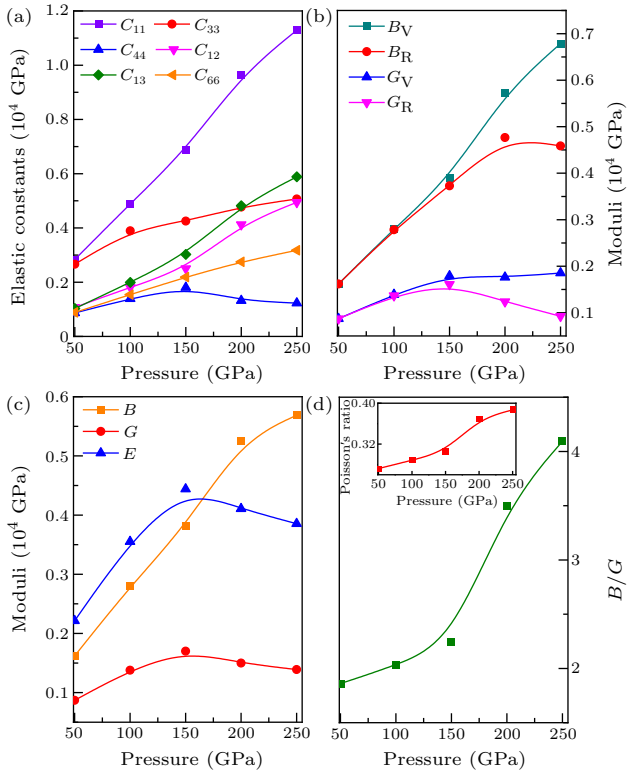


Fig. 4. (a) Elastic constants, (b) bulk modulus (B_V, B_R) and shear modulus (G_V, G_R), (c) Young's modulus E, bulk modulus B and shear modulus G, (d) the Pugh criterion (B/G) and Poisson's ratio as functions of pressure.

3.3. Electronic properties and chemical bonding

The electronic properties of $HfZn_2$ under high pressure are further explored. Figure 5 presents the electronic band structures along the high-symmetry directions in the Brillouin zone and partial densities of states (PDOS) for $Fd\bar{3}m$ and $P6_3/mmc$ phases at different pressures. The overlap between the conduction and the valence bands for the two structures suggests that the above phases are metallic (Figs. 5(a) and 5(c)). The PDOS around the Fermi level is dominated by the Zn-p and Hf-d orbitals for all structures with almost no Hf-s component as shown in Figs. 5(b) and 5(d).

Analyzing the types of chemical bonds for the stable structures is also an important aspect. The electronic localization function (ELF)[24] has become a successful method to characterize the localized distribution of electrons and bonding nature in materials. Typically, ELF values greater than 0.5 indicate localized electrons, corresponding to covalent bonds, while ELF values less than 0.5 suggest delocalized electrons, indicative of ionic bonds. The value 0 refers to very low charge density. From the calculated ELF of $Fd\bar{3}m$ and $P6_3/mmc$ phases (Fig. 6), it is evident that the Hf–Zn bond exhibits ionic character. Then, Bader charge analysis was used to measure the amount of charge transfer from $Fd\bar{3}m$ phase to $P6_3/mmc$ phase at different pressures. It can be observed that each Zn gains about 0.43 electron and 0.40 electron is transferred from Hf for $Fd\bar{3}m$ and $P6_3/mmc$ structure, at 10 GPa and 200 GPa, respectively.

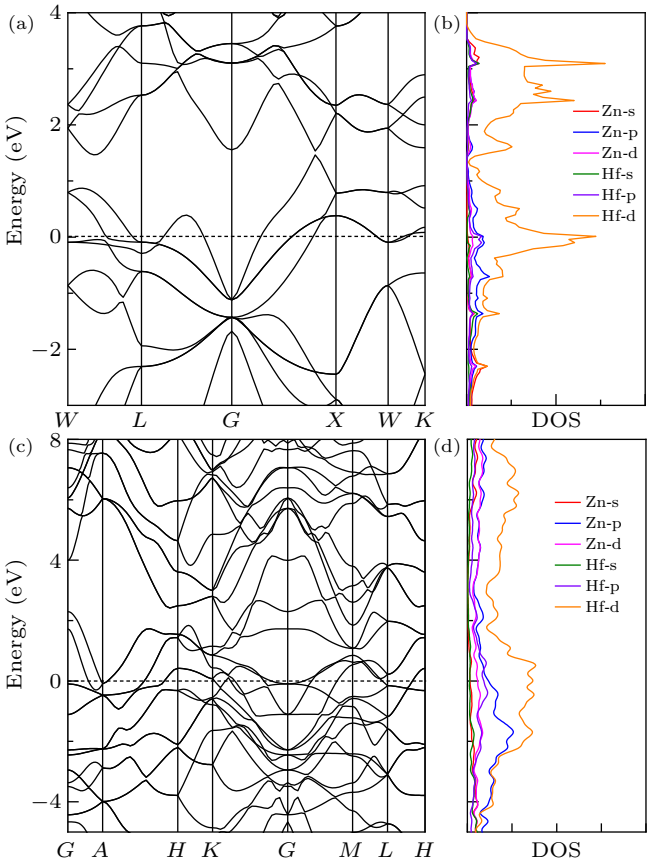


Fig. 5. (a) Electronic band structures and (b) partial densities of states (DOS) of $Fd\bar{3}m$ phase of $HfZn_2$ at 10 GPa. (c) Electronic band structures and (d) partial densities of states (DOS) of $P6_3/mmc$ phase of $HfZn_2$ at 200 GPa.

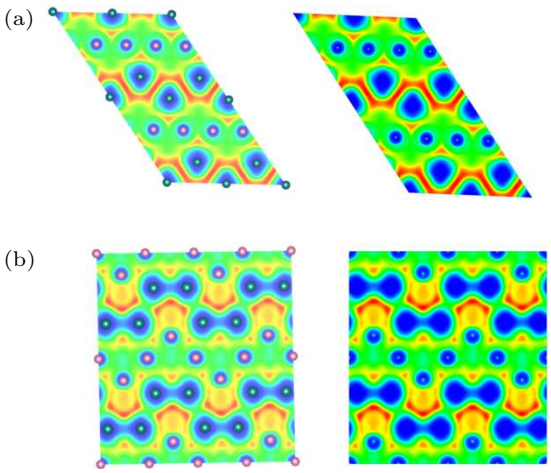


Fig. 6. The ELF of $HfZn_2$ with space groups (a) $Fd\bar{3}m$ at 10 GPa and (b) $P6_3/mmc$ at 200 GPa.

3.4. Superconductivity

To observe the superconductive properties of the $Fd\bar{3}m$ and $P6_3/mmc$ phases for $HfZn_2$ under high pressure, the electron-phonon coupling (EPC) calculations were performed, and the results are shown in Table 2. As the low-pressure phase, $HfZn_2$ with space group $Fd\bar{3}m$ exhibits the highest superconducting critical temperature of 3.89 K at 10 GPa, due to a large electron–phonon coupling parameter λ around 0.74. Although pressure generally enhances logarithmic av-

erage phonon frequency $\omega_{\log}$, which is directly proportional to superconductive critical temperature, pressure significantly suppressed electron–phonon coupling parameter λ of $Fd\bar{3}m$ phase of $HfZn_2$ as shown in Table 1. This suppression originates from a sharp decrease in Fermi surface DOS ($N(E_F)$) from 39.04 eV to 33.81 eV and weakened Hf-d/Zn-p hybridization. Consequently, $HfZn_2$ with space group $Fd\bar{3}m$ at 20 GPa exhibits a superconducting critical temperature of only 0.30 K with λ collapsing to 0.35 and $\omega_{\log}$ rising to 176.86 K. After the transition from $Fd\bar{3}m$ phase to $P6_3/mmc$ phase, the superconducting critical temperature of $HfZn_2$ increases to 0.55 K at 50 GPa. This phase transition reconstructs the Fermi surface, stabilizing λ near 0.37 despite decreasing $N(E_F)$ attributed to Brillouin zone folding that reaggregates Hf-d states near $N(E_F)$ and sustains strong d–p hybridization. Unlike $Fd\bar{3}m$ phase, the superconducting critical temperature of the $P6_3/mmc$ phase is not sensitive to pressure below 150 GPa, they are 0.65 K and 0.41 K at 100 GPa and 150 GPa, respectively. These fluctuations arise from competition between increasing $\omega_{\log}$ from 203.46 K to 256.76 K and declining $N(E_F)$ from 63.91 eV to 48.45 eV. The increase in $\omega_{\log}$ dominates at 100 GPa, resulting in $T_c = 0.65$ K, while $N(E_F)$ loss prevails at 150 GPa, lowering T_c to 0.41 K. The electron–phonon coupling parameter λ is almost unchanged in the pressure range 50–150 GPa. As the pressure is further increased to 200 GPa, the electron–phonon coupling parameter λ suddenly drops to 0.25, triggered by severe Hf-d orbital delocalization ($N(E_F) = 29.08$ eV) that suppresses the electron–phonon matrix elements. As a result, the superconducting critical temperature of $P6_3/mmc$ phase decreases to 0.02 K despite $\omega_{\log}$ reaching 292.66 K.

Table 2. The calculated electron–phonon coupling parameters (λ), the logarithmic average phonon frequency $\omega_{\log}$, electronic density of states at the Fermi level $N(E_F)$ (states/spin/Ry/unit cell), and superconducting critical temperatures T_c of the $Fd\bar{3}m$ and $P6_3/mmc$ phases for $HfZn_2$ at different pressures.

Structures	Pressure (GPa)	λ	$\omega_{\log}$ (K)	$N(E_F)$	T_c (K)
$Fd\bar{3}m$	10	0.74	97.97	39.04	3.89
	20	0.35	176.86	33.81	0.30
$P6_3/mmc$	50	0.37	203.46	63.91	0.55
	100	0.37	231.62	59.11	0.65
	150	0.35	256.76	48.45	0.41
	200	0.25	292.66	29.08	0.02

4. Summary

The study conducted a comprehensive study on the high-pressure phase diagram of $HfZn_2$ using crystal structure prediction based on density functional theory. Our findings revealed a high-pressure $C14$ phase of $HfZn_2$ with the space group $P6_3/mmc$. The $C15$ to $C14$ phase transition of $HfZn_2$ emerges at 20 GPa, and when pressure further increases to 275 GPa, $HfZn_2$ tends to decompose into Hf and Zn. Then we investigated the properties of high-pressure $C14$ phase of $HfZn_2$, including its mechanical, chemical bonding and superconductive properties. We first clarify the mechanical properties of $C14$ phase $HfZn_2$ under pressure. The ratio of bulk modulus and shear modulus (B/G) increases from 1.86 to 4.09 in the pressure range of 50–250 GPa, which indicates that the $C14$ phase of $HfZn_2$ exhibits excellent ductility under high pressure. Moreover, Zn gains about 0.43 electron from Hf at 10 GPa, and pressure facilitates electron transfer from Hf to Zn. The superconducting critical temperature of $C14$ $HfZn_2$ is about 0.55 K in a pressure range of 50–150 GPa. The pressure-induced superconductivity of $C15$ and $C14$ $HfZn_2$ will enhance the fundamental understanding of high-pressure properties of Laves-phase alloys. Elucidating the high-pressure behaviors of the $C14$ and $C15$ phases of $HfZn_2$ will trigger further applications of Laves-phase alloys under extreme conditions.

Acknowledgment

Project supported by the Guangxi Natural Science Foundation (Grant Nos. 2025GXNSFAA069277 and GuikeAD23026204).

References

[1] Liu C T, Zhu J H, Brady M P, McKamey C G and Pike L M 2000 *Intermetallics* **8** 1119
[2] Yang Q S, Ruan B B, Zhou M H, Gu Y D, Ma M W, Chen G F and Ren Z A 2023 *Chin. Phys. B* **32** 017402
[3] Yartys V A and Lototskyy M V 2022 *J. Alloys Compd.* **916** 165219
[4] Santi G, Dugdale S B and Jarlborg T 2001 *Phys. Rev. Lett.* **87** 247004
[5] Jain H and Saad M 1983 *Hyperfine Interact.* **16** 805
[6] Foster K, E H J, G L R and Skripov V A 2000 *Philos. Mag. B* **80** 1667
[7] Sun N, Zhang X, Qin J, Ning J, Zhang S, Liang S, Ma M and Liu R 2014 *J. Appl. Phys.* **115** 083514
[8] Li G J, Shi L T, Hu C E, Cheng Y and Ji G F 2018 *Acta Phys. Pol. A* **133** 1299
[9] Rahman M A, Rahman M A and Rahaman M Z 2015 arXiv:1510.04944 [cond-mat.mtrl-sci]
[10] Rahaman M Z and Rahman M A 2016 arXiv:1605.04841 [cond-mat.mtrl-sci]
[11] Wang Y, Lv J, Zhu L and Ma Y 2012 *Comput. Phys. Commun.* **183** 2063
[12] Glass C W, Oganov A R and Hansen N 2006 *Comput. Phys. Commun.* **175** 713
[13] Oganov A R, Lyakhov A O and Valle M 2011 *Acc. Chem. Res.* **44** 227
[14] Hafner J 2008 *J. Comput. Chem.* **29** 2044
[15] Perdew J P, Burke K and Ernzerhof M 1996 *Phys. Rev. Lett.* **77** 3865
[16] Wang T, Wen M H, Zhang X X, Wang W H, Liu J M, Wang X Y and Li P F 2025 *Chin. Phys. B* **34** 036104
[17] Fan L L, Liu X, Gao C, Liu Z L, Li Y L and Huang H J 2025 *Chin. Phys. B* **32** 079101
[18] Togo A, Chaput L, Tadano T and Tanaka I 2023 *J. Phys.: Condens. Matter* **35** 353001
[19] Giannozzi P, Baroni S, Bonini N, Calandra M, Car R, Cavazzoni C, Ceresoli D, Chiarotti G L, Cococcioni M and Dabo I 2009 *J. Phys.: Condens. Matter* **21** 395502
[20] Mouhat F and Coudert F X 2014 *Phys. Rev. B* **90** 224104
[21] Huang H H, Fan X, Yang G M, Singh D J and Zheng W T 2018 *Comput. Mater. Sci.* **144** 147
[22] Chung D H and Buessem W R 1967 *J. Appl. Phys.* **38** 2535
[23] Sun Z, Li S, Ahuja R and Schneider J M 2004 *Solid State Commun.* **129** 589
[24] Savin A, Nesper R, Wengert S and Fässler T F 1997 *Angew. Chem. Int. Ed.* **36** 1808